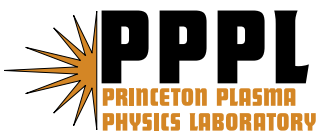

Princeton Plasma Physics Laboratory

PPPL-

PPPL-



Prepared for the U.S. Department of Energy under Contract DE-AC02-76CH03073.

Princeton Plasma Physics Laboratory

Report Disclaimers

Full Legal Disclaimer

This report was prepared as an account of work sponsored by an agency of the United States Government. Neither the United States Government nor any agency thereof, nor any of their employees, nor any of their contractors, subcontractors or their employees, makes any warranty, express or implied, or assumes any legal liability or responsibility for the accuracy, completeness, or any third party's use or the results of such use of any information, apparatus, product, or process disclosed, or represents that its use would not infringe privately owned rights. Reference herein to any specific commercial product, process, or service by trade name, trademark, manufacturer, or otherwise, does not necessarily constitute or imply its endorsement, recommendation, or favoring by the United States Government or any agency thereof or its contractors or subcontractors. The views and opinions of authors expressed herein do not necessarily state or reflect those of the United States Government or any agency thereof.

Trademark Disclaimer

Reference herein to any specific commercial product, process, or service by trade name, trademark, manufacturer, or otherwise, does not necessarily constitute or imply its endorsement, recommendation, or favoring by the United States Government or any agency thereof or its contractors or subcontractors.

PPPL Report Availability

Princeton Plasma Physics Laboratory:

<http://www.pppl.gov/techreports.cfm>

Office of Scientific and Technical Information (OSTI):

<http://www.osti.gov/bridge>

Related Links:

[U.S. Department of Energy](#)

[Office of Scientific and Technical Information](#)

[Fusion Links](#)

Simulation of α -channeling in mirror machines

A. I. Zhmoginov, N. J. Fisch

Princeton Plasma Physics Laboratory, Princeton, NJ 08543, USA

Abstract

Applying α -channeling techniques to mirror machines can significantly increase their effective reactivity, thus making open configurations more advantageous for practical fusion. A large fraction of α particle energy can be extracted using rf waves. Effects employed to cool α particles can also in principle be used to heat the fusion ions; the possibility to design a configuration of rf waves which could be used to perform both tasks is demonstrated.

I. INTRODUCTION

Mirror machines and related open-trap devices have several advantages over tokamaks, such as simplicity, high- β , and steady-state operation. Unfortunately, the prospects for fusion based on these concepts are dimmed by their low Q-factor, the ratio of fusion power produced to circulating power employed [1, 2]. Increasing the Q-factor could enhance significantly the prospects of mirror fusion. By analogy with the alpha channeling effect in tokamaks [3], α -channeling in mirror machines could be one such enhancement [4, 5]. Like in tokamaks, the Q-factor of the mirror machine might be increased by channeling energy by waves from α particles to fuel ions [6–8], and quickly removing fusion ash which takes up valuable electric potential, thereby diminishing the number of confined fuel ions. Maintaining ion and electron temperature disparities can be useful in mirror machines [9, 10], and both the temperature disparities and the reducing of the fusion ash increase the effective fusion reactivity much like in tokamaks [11]. The channeling of the alpha power in one simple mirror configuration at ignition has been estimated [4] to increase potentially the effective fusion reactivity by a factor of 2.8.

The α -channeling effect in a mirror machine might be implemented by arranging regions with high- m azimuthally-propagating electrostatic waves in the ion-cyclotron range of frequencies (like mode-converted ion Bernstein wave [12, 13]) along the device axis (see Fig. 1). The α particles that resonantly interact with such waves are restricted to thin paths in the velocity-configuration space, or diffusion paths [3] (see Fig. 2). Previous calculations [4, 5] of α particle diffusion along these paths assumed that the diffusion paths were of vanishing thickness and only the asymptotic time behaviour of the particles was considered.

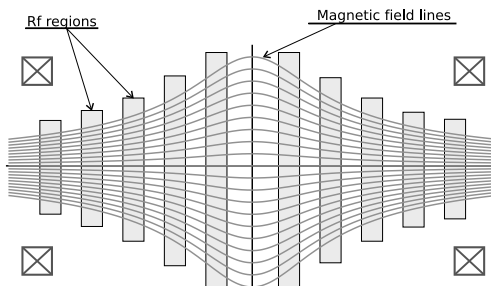


FIG. 1: Arrangement of regions (shown with grey bars) with high- n azimuthally propagating radially-localized electrostatic waves in the ion cyclotron range of frequencies.

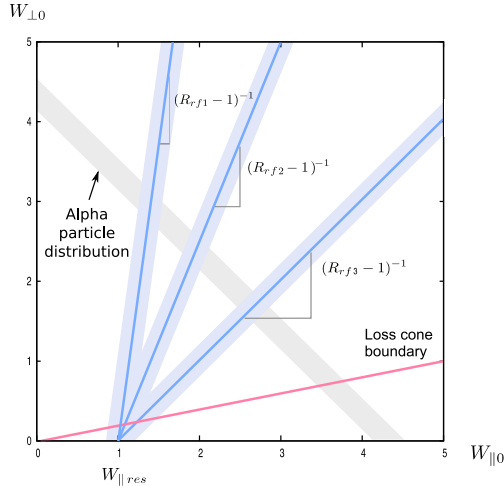


FIG. 2: (Color online) Implementation of α -channeling in mirror machines. Configuration of diffusion paths in the midplane energy space $W_{\parallel 0}$ - $W_{\perp 0}$ used for α particle cooling; finite widths of diffusion paths affect exit energy uncertainty and lead to an intersection of paths what isotropizes diffusion tensor in a vicinity of a loss cone.

A finite width of the diffusion paths captures α particles within the full accessible range of pitch-angles, which is helpful, but it makes uncertain the exit energy, since diffusion paths can intersect. Besides depending on the average energy of the exiting α particles, the efficiency of α -channeling also depends on the particle extraction or channeling time. The extraction time needs to be much smaller than the collisional energy relaxation time for effective channeling.

In this work we numerically study the particle distribution function evolution in a mirror machine of finite length under the influence of multiple rf regions. We consider the non-ideal effects of finite diffusion time and intersection of diffusion paths. Although a strict optimization was not performed, the possibility to extract more than 60% of energy of resonant α particles in a practical system design is simulated. It is also shown that wave-particle interactions can be used to couple energy extraction from α particles with the plasma injection accompanied by heating of fuel ions.

The paper is organized as follows: In the Sec. II we describe the single particle motion. Sec. III describes the particle distribution function evolution. Sec. IV introduces the computational method used for the numerical simulations of α -channeling described in Sec. V. Sec. VI discusses hot fuel ion pump-out by rf regions employed for α -channeling. Sec.

VII summarizes our conclusions. Appendix A describes analytical estimates for diffusion path characteristics.

II. SINGLE PARTICLE MOTION

The single particle motion in the simple mirror machine under the influence of rf fields can be described by coupled position-velocity diffusion in midplane coordinates [4]. To calculate the finite diffusion time effects, however, the magnitude of the diffusion coefficient enters importantly; following [14–16] we rederive the diffusion coefficient along those paths. Consider an axially symmetric magnetic mirror trap with a system of localized rf regions located along the device axis. Suppose that the radial size of the system is much smaller than its longitudinal scale length L , so that a paraxial approximation for the magnetic field can be used: $\mathbf{B} = rB'_z(z)/2 + B_z(z)\hat{\mathbf{z}}$. Electrostatic waves localized in layers $z_i < z < z_i + l^i$ of width l^i thin compared to the device size L , propagate longitudinally and azimuthally. In each layer the wave is described by the scalar potential $\varphi^i = \varphi_0^i(r, z) \cos(-\omega^i t + k_z^i z + m^i \psi)$ where i is a layer number, ψ is an azimuthal angle and $\hat{\mathbf{z}}$ is an axis directed along the axis of symmetry of the system.

The motion of a charged particle in the rf region is governed by equation: $m\dot{\mathbf{v}} = ec^{-1} \mathbf{v} \times \mathbf{B} + q\varphi_0 \mathbf{k} \sin(-\omega_0 t + k_z z + m\psi)$, where $\mathbf{k}_\perp = \hat{\psi} m/r$. Renormalizing time $\tau = t\Omega_0$ and gyrofrequency $\Omega = eB/(mc\Omega_0)$ to the midplane ($z = 0$) gyrofrequency Ω_0 and magnetic field $\mathbf{b} = \mathbf{B}/B_0$ to the midplane magnetic field B_0 , we obtain an equation for renormalized velocity $\mathbf{u} = \mathbf{v}/\Omega_0$:

$$\frac{d\mathbf{u}}{d\tau} = \mathbf{u} \times \mathbf{b} + \mathbf{k} f_0 \sin(-\omega\tau + k_z z + m\psi), \quad (1)$$

where $\omega = \omega_0/\Omega_0$ and $f_0 = q\varphi_0/m\Omega_0^2$.

Suppose that a particle is close to the axis, $r \ll L$, yet $r \gg \rho$. Suppose also that there can be just a single resonance on the whole length of the rf region; then the particle motion can be approximately described by [17–19]:

$$\frac{d\delta}{dz} \approx -\frac{f_0 k_z}{u_{\parallel 0}} J_{l_r}(m\rho/r) \sin(\phi + l_r \alpha_0) + \frac{df_0/dz}{u_{\parallel 0}} J_{l_r}(m\rho/r) \cos(\phi + l_r \alpha_0), \quad (2)$$

$$\frac{d\phi}{dz} = (\omega - k_z u_{\parallel 0} - l_r \Omega)/u_{\parallel 0} - (\omega - l_r \Omega)\delta/u_{\parallel 0}^2, \quad (3)$$

$$dE/d\delta \approx \omega/k_z, \quad (4)$$

$$\frac{dr}{dE} \approx -\frac{m}{r\omega\Omega}, \quad \text{or} \quad \frac{dr^2}{dE} \approx -\frac{2m}{\omega\Omega}, \quad (5)$$

where $\delta = u_{\parallel} - u_{\parallel 0}$ is a small parallel velocity perturbation, $E = u^2/2$, $u_{\perp}^2 = u^2 - u_{\parallel}^2$, $\rho = u_{\perp}/b$, α_0 is the initial gyroangle, l_r is a resonance number and $u_{\parallel 0}$ is an unperturbed parallel velocity equal to $\sqrt{2E - 2\mu b(z)}$.

Eqs. (2-5) describe single particle motion within each rf region. Typically, each particle bounce results in a random excursion along the diffusion path given by Eqs. (4) and (5) and proportional to δ . Eqs. (4) and (5) show that the diffusion path intersects the axis $W_{\perp}^0 = 0$ at $W_{\parallel}^0 = (\omega - l\Omega)^2/k_z^2$ and that the slope of the path is

$$W_{\perp}^0/W_{\parallel}^0 \approx \frac{1 + (1 - l\Omega/\omega)}{(b - 1) - (1 - l\Omega/\omega)} \approx (b - 1)^{-1},$$

as used in Ref. [4]. The diffusion coefficient describing the particle random walk follows from Eq. (2), consistent with Refs. [14–16]:

$$D_E = \Delta E^2/\Delta\tau_{\text{bnc}} \sim f_0^2(r)\sqrt{bE}J_l^2(\rho bE/r), \quad (6)$$

where $\Delta\tau_{\text{bnc}} = 2\pi L/u_{\perp}$ stands for particle bounce time. Interestingly, the diffusion coefficient reaches zero in an infinite number of points along the diffusion path. The zeroes of the diffusion coefficient can be important because they limit the diffusive particle heating.

III. PARTICLE DISTRIBUTION EVOLUTION

To describe the distribution function evolution for stochastically moving particles we use a Monte-Carlo algorithm. Neglecting the dependence of $k_{\perp} \approx (m/r_0)(1 - \Delta r/r_0)$ on the radial particle excursion Δr , for each passage of the particle through some rf region, the midplane velocity and time increments are calculated as

$$\mathbf{u}_{n+1} = \mathbf{u}_n + \mathbf{f} + \hat{\mathbf{d}}\mathbf{w}, \quad (7)$$

$$\tau_{n+1} = \tau_n + \Delta\tau(\mathbf{u}), \quad (8)$$

where $\mathbf{f} = \langle \Delta\mathbf{u} \rangle$ and $\hat{\mathbf{d}} = \langle \Delta\mathbf{u} \Delta\mathbf{u} \rangle$ are calculated using Eq. (1) and can be visualized with help of *diffusion diagrams* (see Fig. 3); $\Delta\tau$ is the time the particle spent within the rf field and \mathbf{w} is a two-dimensional random vector, such that $\langle w_i \rangle = 0$ and $\langle w_i^2 \rangle = 1$. Since diffusion occurs essentially along a 1-D path, it can be visualized as a vector field in which the

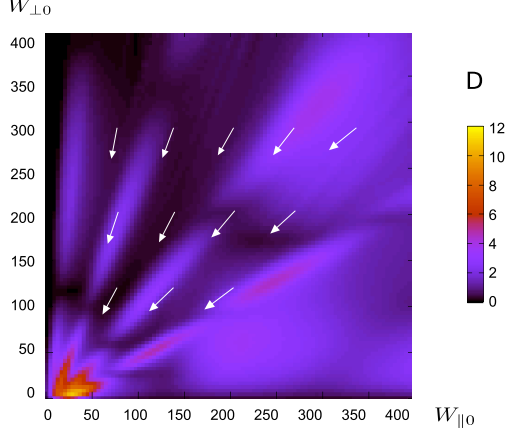


FIG. 3: (Color online) Diffusion diagram for the arrangement of paths shown on Fig. 2. Arrows indicate the direction of the strongest diffusion, color stands for corresponding diffusion coefficient. The area with largest D is influenced by several diffusion paths.

direction of the vector is taken along the path and the magnitude of the vector is taken to be the magnitude of the diffusion coefficient. In principle, particles with regular orbits can be accounted for by setting $\hat{\mathbf{d}}$ and \mathbf{f} to 0. Strictly speaking, the time $\Delta\tau$ in Eq. (8) has a random component too, yet it only contributes a small correction of order $(d/u)(L_{\text{wl}}/L_{\text{sys}})$ to the total time, where L_{wl} is the total length of all wave regions and L_{sys} is the full mirror length. The change of k_{\perp} seen by a particle moving along the diffusion path can be accounted for semi-analytically by keeping track of the particle radial displacement $\Delta r^2 \sim -2m(\omega\Omega)^{-1}\Delta E$ and scaling the particle energy excursion according to $\Delta E_n \sim f_0(r)J_{l_r}(m\rho/r)$.

Assuming that the average velocity increments (7) are much smaller than the characteristic velocity scales of the particle distribution function, Eq. (7) can be rewritten as an Itô Stochastic Differential Equation [20]:

$$\mathbf{u}(\tau_n + \Delta\tau) = \mathbf{u}(\tau_n) + \mathbf{F}(\mathbf{u}(\tau_n))\frac{\Delta\tau}{\tau_{\text{bnc}}} + \hat{\mathbf{D}}(\mathbf{u}(\tau_n))\tilde{\mathbf{w}}(\Delta\tau/\tau_{\text{bnc}})$$

where $\mathbf{F} = \langle \Delta\mathbf{u}_{\text{bnc}} \rangle$ and $\hat{\mathbf{D}} = \langle \Delta\mathbf{u}_{\text{bnc}}\Delta\mathbf{u}_{\text{bnc}} \rangle$ represent averages of the velocity change on a bounce time $\tau_{\text{bnc}}(\mathbf{u})$, and $\tilde{\mathbf{w}}$ being a two-dimensional Wiener process. The particle distribution evolution can then be described by the Itô Fokker-Planck equation:

$$\frac{\partial p}{\partial \tau} = - \sum_i \frac{\partial}{\partial u_i} \left(\frac{F_i p}{\tau_{\text{bnc}}} \right) + \frac{1}{2} \sum_{i,j} \frac{\partial^2}{\partial u_i \partial u_j} \left[\frac{p}{\tau_{\text{bnc}}} \left(\hat{\mathbf{D}} \hat{\mathbf{D}}^T \right)_{ij} \right], \quad (9)$$

where $p(\mathbf{u}, t)$ is the particle distribution function in the 2-D midplane velocity space. This model does not account for particle collisions. Our assumption is that collisions may be

TABLE I: Dependencies $n_{\text{loss}}(t)$ and $E(t)$ for resonant particles calculated using both random-walk equations and exact 6D particle motion Eq. (1).

t , ms	3	6	12	25	50
$n_{\text{loss walk/exact}}$, %	7.5 / 9.0	25.6 / 29.4	48.3 / 49.7	69.2 / 74.3	83.3 / 86.3
$E_{\text{walk/exact}}$, MeV	3.45 / 3.40	3.19 / 3.13	2.92 / 2.85	2.59 / 2.38	2.23 / 2.04

neglected since the collision frequency is much smaller than the characteristic inverse time scale in the regimes of interest. Note that this analysis assumes that particles are well-described by diffusion equations. More generally, the particle motion in a mirror machine geometry in the presence of rf waves can be treated by examining the Poincare map as particles cross the central cross-section, wherein both stochastic regions and invariant tori can be distinguished [21–25]. However, here we simply assume that the preponderance of particles are in fact stochastic, either because of a variety of practical aspects: the nonlinear wave effects [26, 27], a small number of collisions, or wave incoherence.

IV. COMPUTATIONAL METHOD

Describing the particle motion as a random walk process is a major computational simplification. To verify that a simulation based on Eqs. (7) and (8) describes the particle distribution function evolution adequately, even assuming wave coherence and even in the absence of collisions, we compared our Monte-Carlo results with the exact solution of Eq. (1). The number of particles which left the system n_{loss} , the average energy of all particles E (including those escaped), and the characteristic shape of the particle distribution were compared for different times t for resonant particles diffusing along a single path. The good agreement shown in Table I between dependencies obtained using Monte-Carlo and Eq. (1) suggests that the random walk process can be used to describe adequately the particle distribution evolution. Nonetheless, in order to verify our other results, exact solutions for small number of particles were tracked in all further simulations.

The approximate Eqs. (2), (3) and (4) can be used to estimate resonant particle diffusion tensor $\hat{\mathbf{d}}$ and determine characteristic parameters of the diffusion paths. These approximations will be most precise for short times; large deviations in particle distribution evolution

are expected when long-time dynamics in a system with several rf waves is considered.

The rf region parameters are chosen using estimates outlined in Appendix A. First, the inner radial profile boundary r_0 and ion-cyclotron resonance number l_r are picked. The designed diffusion path slope defines b at the rf region location and the azimuthal wave number m is chosen to optimize the diffusion coefficient distribution along the path $D_E \sim \sqrt{E} J_{l_r}^2(m\rho/r)$. The designed path width defines k_{\parallel} through Eq. (A-4). Even though the diffusion path width should be smaller for more effective α -channeling, it can not be chosen arbitrarily small, being limited by Eq. (A-4) and condition $k_{\parallel} \ll \omega/u_{\parallel\text{res}}$ which is necessary for small particle parallel velocity perturbation. The wave frequency ω is chosen to select a certain resonant parallel velocity $u_{\parallel\text{res}} = (\omega - l_r\Omega)/k_{\parallel}$ and the rf region length is picked to be smaller than l_{res} defined by Eq. (A-3) and smaller than $k_{\parallel}u_{\parallel}/(b'L)$ to avoid resonance with particles reflected inside the wave.

The number of rf regions in the system is limited by the requirement to capture α particles within a whole accessible range of pitch angles and by the length of the system. The amplitudes of the rf regions determine the α particle diffusion rate. There are also limitations imposed on these amplitudes. The waves of course are derived under the condition that $e\varphi \ll kT$ so that the perturbation of plasma density is small, i. e., $n \approx n_0 \exp(-e\varphi/kT)$. A more stringent limitation arises from the effect on the fuel ions; as discussed in Sec. VI, using high-amplitude rf waves can lead to fuel ion pump-out even if the interaction is non-resonant. Thus, for intersecting multiple waves, the fuel ion residence time may impose additional limitations on practical rf wave amplitudes.

V. SIMULATION RESULTS

To explore computationally the feasibility of cooling down 3.5 MeV α particles, we varied the diffusion paths in the midplane energy space. The configuration consisted of thin diffusion paths with the same resonant velocity, but different slopes in $W_{\parallel} - W_{\perp}$ space (Fig. 2). Diffusion paths with various slopes were used to diffuse α particles within a wide range of pitch-angles. The choice of resonant velocity was based on avoiding expulsion of fuel ions and maximizing the extracted energy for the α particles.

For efficient α -channeling, α particle heating along the diffusion path should be limited. The issue with unlimited heating is not that the particle gains unlimited energy; rather the

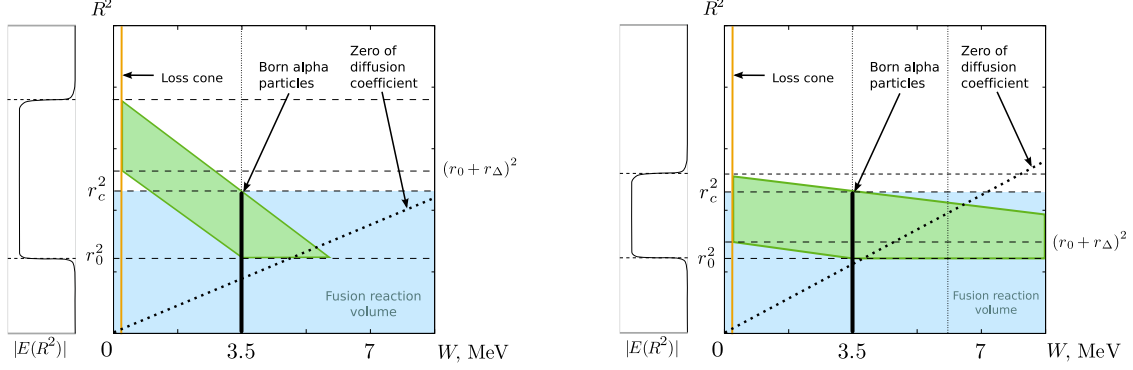


FIG. 4: (Color online) Diffusion paths in the coupled configuration-energy space in two regimes: (a) $r_\Delta \sim r_c$ with limitation at low wave radial profile boundary r_0 and (b) $r_\Delta \ll r_c$ with limitation at $k_\perp \rho \approx m\alpha\sqrt{E}/r = z_1$, where z_1 stands for first zero of $J_l(z)$ and α is a constant depending on $b(z)$.

issue that in the finite time scale associated with its collisional slowing down, the α particle is not extracted. A limitation can be imposed through the radial particle excursion $r_\Delta > 0$, that is coupled to energy excursion ΔE . Suppose the α particles are born in a hot device center of radius r_c . If $r_\Delta \gtrsim r_c$, the limitation of α particle penetration into the device center is caused by approaching lower wave radial profile boundary r_0 (see Fig. 4a). When $r_\Delta \ll r_c$, the majority of α particles can be heated to very high energies while remaining in the rf region (see Fig. 4b). The effects which can limit heating in this case include: (a) the vanishing of diffusion coefficient $D_E \sim \sqrt{E}J_l^2(m\rho/r)$; (b) leaving the resonance $\omega - k_\parallel u_\parallel - l\Omega \approx 0$ when a change of the particle energy ΔE leads to a significant parallel velocity change $\Delta u_\parallel \sim (k_\parallel/\omega)\Delta E$.

We simulated two device designs. In both designs, the magnetic field was 2 T at the midplane with parabolic axial profile $b = 1 + z^2/L^2$, and with mirror ratio $R = 5$; in the longer design, L was taken as 20 m and in the smaller, as 10 m. Eight waves with longitudinal wave profile $|E(z)| \sim E_0 \sin[\pi(z - z^i)/l^i]$, $E_0 \sim 200$ to 300 kV/m, $r_0 \sim 1$ m, $m \sim 40$ to 70 and $k_\parallel \sim 0.04$ to 0.1 cm^{-1} were placed along the system axis. These waves perturbed the density of 20 keV plasma by less than 5%. Because the effective resonance layer length l_{res} defined by Eq. (A-3) is proportional to \sqrt{L} , increasing the length of the system and choosing $l^i \approx l_{\text{res}}$, while keeping other wave parameters unchanged, results not only in enhanced particle diffusion, but also in smaller diffusion path widths defined by Eq.

TABLE II: Numerical simulation results for both device designs. Here n_{loss} is the amount of α particles initially resonant with waves (approximately 70% of all trapped α particles interacting with waves) that leave the system in time t , E is the average particle energy for both left particles and particles remaining in the system, E_{loss} is an average energy of the exiting particles.

t , ms	10	25	50	100	150	300
$L = 10$ m, Bessel zero limitation						
n_{loss} , %	22.0	32.2	42.2	51.4	56.6	65.1
E , MeV	3.0	2.9	2.9	2.8	2.6	2.5
E_{loss} , MeV	1.06	0.99	0.94	0.88	0.85	0.85
$L = 20$ m, Bessel zero limitation						
n_{loss} , %	24.1	35.6	46.7	56.7	62.3	72.0
E , MeV	2.7	2.6	2.4	2.3	2.2	2.1
E_{loss} , MeV	0.91	0.88	0.84	0.75	0.76	0.77
$L = 20$ m, radial limitation						
n_{loss} , %	31.1	53.3	66.7	71.1	75.5	80.2
E , MeV	2.7	2.3	2.1	1.9	1.8	1.6
E_{loss} , MeV	0.96	0.84	0.76	0.63	0.6	0.55

(A-4). Therefore, to avoid diffusion paths near $u = 0$, larger resonant velocities were chosen in the system with $L = 10$ m; this resulted in higher average output α particle energy and smaller α -channeling efficiency (see Table II).

The numerical simulations in the longer device were conducted for two regimes (see Table 2): (a) $r_{\Delta} \ll r_c$ with limitation by a zero of a Bessel function and (b) “radially limited” paths when $r_{\Delta} \gtrsim r_c$. In the system with paths limited by zeros of Bessel functions, particles left the device slowly because the diffusion coefficient never vanishes exactly on the path. Some particles passed the point where $D_E \approx 0$, becoming trapped above it. The average particle energy over long times was also found to be higher because particles trapped over $D_E \approx 0$ could be heated to rather high energies. Further numerical simulations of α -channeling in the longer device confirmed the possibility to extract more than 60% of energy of resonant α particles in 300 ms. These simulations employed waves that perturb the plasma density

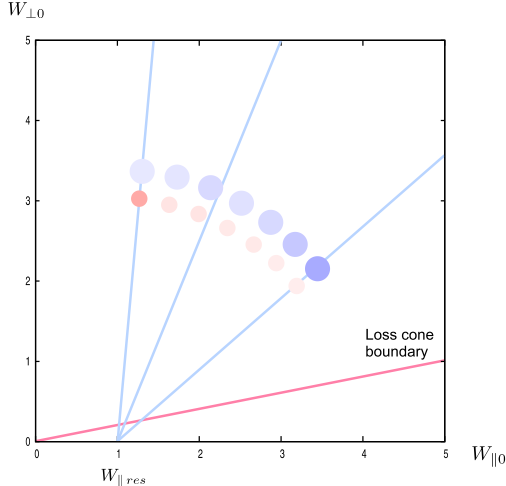


FIG. 5: (Color online) Diagram representing dependence of channeling time (small circle) and average output energy (large circle) of alpha particles on their initial pitch angle. Darker colors stand for larger values.

by less than 5%. Fig. 5 shows the dependence on the initial particle pitch angle of the average output energy and the number of particles leaving the system in a given time. It was observed that particles near the loss cone boundary tend to leave the system quicker, but with higher values of output energy, than do the more deeply trapped particles. Also, most of α particles leave the system on a time scale much less than the characteristic time of the α particle collisional slowing down, that is, of order of a second, confirming that the collisionless equations describe the particle density evolution adequately.

In order to affect primarily the particle perpendicular energy and to couple large radial diffusion to the energy diffusion, waves with finite azimuthal wave numbers are necessary. Low azimuthal wave number waves in ion-cyclotron range of frequencies have been coupled into mirrors [28–34]. The excitation of the higher azimuthal wave number waves required for effective α -channeling might be achieved through mode conversion.

For a system with several rf regions with amplitudes $E_0 \sim 250$ kV/m, α particles leave the system quickly. For lower wave amplitudes, many rf regions would be needed to retain the short exit times. Thus, by decreasing wave amplitudes and increasing the number of rf regions and the device volume they affect, it is possible to retain the overall wave energy and α -channeling efficiency. Additional techniques for increasing α -channeling efficiency for fixed wave amplitudes include: use of higher cyclotron resonances, but lower resonant velocities;

and waves with higher azimuthal wave numbers. The wave parallel resonant velocity, which determines the maximum possible energy extracted from α particles (see Fig. 2), must be chosen to avoid resonant interaction with fuel ions. As discussed in Sec. 6, higher ion-cyclotron resonances diminish the characteristic ion diffusion rate, allowing a smaller wave parallel resonant velocity, thus improving the α -channeling efficiency. A second technique is to decrease α -channeling time by improving α particle heating limitation along the diffusion path, using waves with higher azimuthal wave numbers. While the azimuthal wave number is increasing, the point where $D_E \approx 0$ moves towards the origin along the diffusion path. Once the zero of D_E passes $E_0 = 3.5$ MeV, the α particle extraction is nearly stopped. To avoid vanishing of D_E along the diffusion path, two almost identical decorrelated rf regions with large, but different azimuthal wave numbers might be employed.

Simulations for the system of 8 high- m rf regions with $l = 3$ and $E_0 \sim 150$ kV/m showed that more than 60% of energy of all resonant α particles could be extracted in 300 ms. The same α -channeling efficiency was simulated for 16 waves with $E_0 \sim 100$ kV/m. Extrapolating these results, the same efficiency is expected for a system of 40 rf regions with $E_0 \sim 60$ kV/m and 60 rf regions with $E_0 \sim 50$ kV/m. Any further increase of the number of rf regions is limited by the length of the device.

The injection of plasma in mirror machines for fueling can also be approached using rf waves [15, 35]. In simulating fuel injection and heating with the same waves used also for α particle energy extraction, two system designs were considered.

In the first configuration, a high-density ion source of cold fuel ions was located near the trapped-passing boundary. Since the diffusion paths connect particles on the loss cone near the cold device periphery with deeply trapped particles in the hot center (see Fig. 6a), this results in a population inversion along the path for both ions and α particles [4]. An ion injected on the path passes through the whole device, interacting with all rf regions situated along its length. The velocity excursion, upon interaction with the resonant wave, can cause it to either become more deeply trapped, or to leave the device. If the ion stays in the device after a single pass, the process repeats until the particle leaves through the loss cone or until it gains substantial energy and fuses. The ion injection at the loss cone is most efficient if the source energy consumption is small compared to the energy of heated fuel ions. This is achievable when the energy of injected, but detrapped, particles is recycled. A possible method might be to use an electrostatic particle traps at both ends of the device (see Fig.

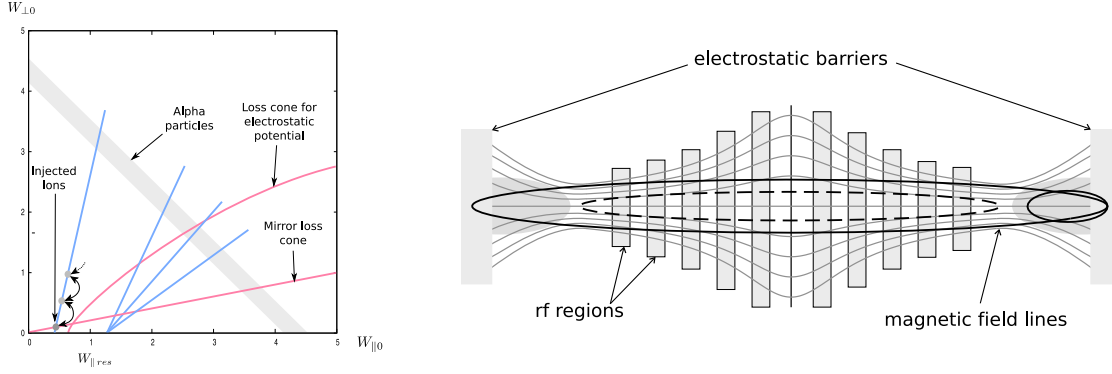


FIG. 6: (Color online) Configuration used for ion injection with the source located on the loss cone: (a) diffusion paths in the midplane energy space, ion velocity excursions are shown schematically with gray circles; (b) proposed device design; three ion trajectories are shown: trajectories of the ion with velocity above the loss cone, trapped in the smaller volume between the mirror and the electrostatic barrier (smaller solid ellipse) and between the magnetic mirrors (dashed ellipse); trajectory of the ion below the loss cone, passing through the whole device and being reflected from the electrostatic barriers (larger solid ellipse).

6b). A cold ion trapped in the smaller region between the magnetic mirror and electrostatic potential barrier may penetrate into the central plug with velocity slightly above the loss cone. If the low-energy particle is not trapped or if it detraps after some period of time, it gets reflected by the electrostatic potential, thus retaining its energy and having a chance to be trapped again.

In the second configuration, ions were injected above the loss cone and diffused along the path limited below the injection point (see Fig. 7a), in order to trap and heat the majority of the injected ions while still extracting α particles.

The possibility to heat fuel ions, transporting them deeper into the mirror machine, and yet cool α particles along the same diffusion path was demonstrated in simulations for both device designs. The characteristic time of ion diffusion along the path was found to be approximately equal to 300 ms. Numerical simulations for configuration with ion injection over the loss cone showed that the average energy of injected ions increased from 20 keV to 80 keV in 100 ms, while only approximately 3% of them escaped the device following other diffusion paths. The loss of the average α particle energy on the same time scale exceeded 400 keV. The time over which half of the injected ions left the device was found to exceed

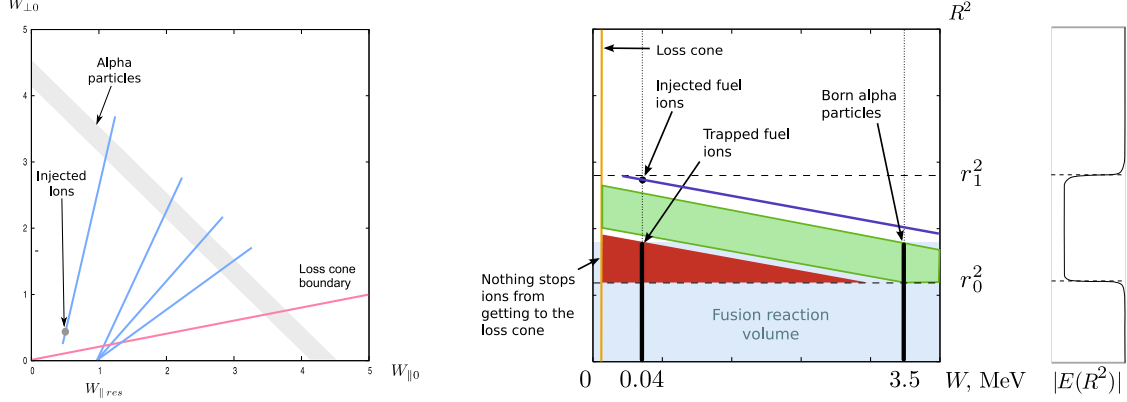


FIG. 7: (Color online) Arrangement of diffusion paths allowing to heat ions by the same wave which is used to cool down α particles: (a) diffusion paths in the midplane energy space; (b) diffusion paths in the coupled configuration-energy space, injected ions are limited at $r = r_1$, α particles and trapped fuel ions with $r > r_0$ escape the system through the loss cone.

1 s.

Despite these promising simulation results, both of the ion injection schemes have certain shortcomings. In both designs, the injected ions can be overheated, reaching energies up to 1.7 MeV. This would not only lower the effective DT fusion reaction cross section relative to its maximum value at $E \sim 70$ keV, but also not optimally employ the rf wave energy. Collisions and other collisionless effects not considered here might, however, limit the heating. Utilization of high-density ion source and trapping escaped ions in the first configuration also imposes additional engineering challenges. The shortcoming of the second injection scheme is the possible interaction of employed rf waves with the trapped fuel ions (see Fig. 7b). However, a wave with $k_{\parallel} = k_{\parallel}(r)$ with a larger resonant parallel velocity near the center, might avoid this interaction.

VI. ION EJECTION BY RF WAVES

One of the major concerns in coupling waves in the ion-cyclotron range of frequencies into mirror machine plasmas is the fuel ion pump-out [36–39]. In Ref. [39], for instance, an increase of ion loss rate was found to correlate with emergence of Alfvén ion cyclotron wave, whose diffusion path connected ions with large pitch angles with the loss cone boundary. Despite using non-resonant rf waves in the present study, the numerical simulations of the

fuel ion distribution evolution in the first device design, discussed in Sec. V with $L = 20$ m, showed that the ion lifetime was approximately equal to 50 ms, corresponding to several hundred bounces in the device. Note that even though the number of bounces is close to those obtained in early works on rf plasma pump-out by DCLC instability [37], in our simulations waves with 100 times larger amplitudes were employed. This smaller pump-out is due to the fact that although nonresonant diffusion takes place, it is much less effective than diffusion by resonant waves.

The characteristic ion velocity excursion in a single pass through the rf region depends on the amplitude of the resonant longitudinal wave harmonic with $k_{\parallel} \approx (\omega - l\Omega)/u_{\parallel}$. The parallel resonance velocities of the diffusion paths were chosen to exceed the fuel ion thermal velocity, thereby avoiding such resonances. However, the longitudinal spectrum of the wave with profile $|E(z)| \sim E_0 \sin[\pi(z - z^i)/l^i]$ had long $\sim 1/k_{\parallel}^2$ tails, resulting in a relatively low ion confinement time. To avoid the long tails, smooth wave profiles with an exponentially decaying spectrum were used and numerically verified to allow better ion confinement, reaching 200 ms. Any further increase of ion time of life by increasing $k_{\parallel}l^i$, thus making the wave spectrum narrower, is limited by the magnetic field gradients, which broaden the resonance. If at some point $z = z_0$ of the rf region, the resonance condition is satisfied for α particles, then $\omega - k_{\parallel}u_{\parallel\alpha} - l\Omega \approx 0$, and at the point $z = z_0 + \Delta z = z_0 + k_{\parallel}u_{\parallel\alpha}/(l\Omega')$, the resonance condition is satisfied for cold ions, thus limiting the rf region length by $l^i \ll \Delta z$.

Besides diminishing ion ejection by using non-resonant rf waves, ion ejection can also be avoided by making the diffusion coefficient for ions vanishingly small near the point where the ions would be ejected, i. e. at low energy, where $k_{\perp}\rho_i < 1$. If $k_{\perp}\rho_i \lesssim 1$, where ρ_i is a characteristic ion gyroradius, ion energy diffusion coefficient $D_E \sim \sqrt{E}J_l^2(k_{\perp}\rho_i) \sim \sqrt{E}(k_{\perp}\rho_i)^{2l}$ can be diminished by using higher cyclotron resonances. The use of waves with $l = 3$ to 5 was shown numerically to further increase ion time of life to several seconds, while retaining the α -channeling efficiency.

The use of the rf waves for injecting the fuel ions and heating those ions is only one of the possible dual uses for the waves that accomplish the α -channeling. Other uses might be to create transport barriers [40] or to maintain a sloshing ion distribution [41]. In either case, if the rf waves are amplified by cooling the α particles, the energy requirement to achieve these uses becomes small. Although it is beyond the scope of this paper to suggest specific waves to accomplish these effects, it is anticipated that the effect would be best

be accomplished by making use of a lightly damped mode in the ion cyclotron range of frequencies [31, 42, 43].

VII. CONCLUSIONS

A multidimensional parameter space, comprised of parameters describing system geometry and individual rf regions, was considered in simulating the α -channeling effect in a simple mirror. For suitable parameter choices, more than 60% of energy of all resonant trapped α particles can be extracted in 300 ms by 8 regions with rf waves, perturbing the plasma density by less than 5%. The further increase of α -channeling efficiency in this configuration is limited by several effects, including the length of the system (which affects α particle diffusion rate and diffusion path width) and wave amplitudes. The wave amplitude is limited by both nonlinear effects and the ion pump-out effect [36, 37]. By employing several rf regions, waves with smooth profiles and higher cyclotron resonances, we showed that trapped fuel ions are not untrapped (collisionlessly) for seconds, while the α particles are extracted in a fraction of a second. To decrease further the rf wave amplitudes while retaining the α -channeling efficiency, several complementary techniques were suggested. More numerous rf regions are helpful; using 40 waves with $E_0 \sim 60$ keV/m should give a high α -channeling efficiency.

We also simulated how ions, injected at the device periphery, can be heated by the same wave which was used to cool down α particles. Two ion injection techniques were proposed. In the first scheme, the ion heating is accomplished by placing a high-density ion source at the trapped-passing boundary and introducing a diffusion path connecting particles on the loss cone at the cold device periphery with the deeply trapped particles in the hot center. In the second scheme, ions are injected above the loss cone and then heated along the diffusion path, but the wave diffusion is small between the injection point and the trapped-passing boundary. Both schemes have similar characteristic ion heating times and accessible ion temperatures, but their implementations impose different engineering challenges.

VIII. ACKNOWLEDGMENTS

This work was supported by DOE Contracts No. DE-FG02-06ER54851 and DE-AC0276-CH03073.

APPENDIX A: ANALYTICAL ESTIMATES FOR DIFFUSION PATH CHARACTERISTICS

In this appendix we show that Eqs. (2) and (3) can be treated analytically in two opposite regimes of strong and weak magnetic field inhomogeneity. We derive characteristic properties of wave-particle interaction which were used to design a system of rf regions in the first case and discuss application of separatrix crossing theory [44, 45] in the opposite regime referring to Refs. [46–48], where particle interaction with only a finite band-width wave was considered.

Eqs. (2) and (3) can be rewritten in a Hamiltonian form:

$$H = \frac{(\omega - k_z u_{\parallel} - l_r \Omega(z))\delta}{u_{\parallel}} - \frac{(\omega - l_r \Omega(z))\delta^2}{2u_{\parallel}^2} - \frac{f_0 k_z}{u_{\parallel}} J_{l_r}(m\rho/r) \cos(\phi + l_r \alpha_0) - \frac{f'_0(z)}{u_{\parallel}} J_{l_r}(m\rho/r) \sin(\phi + l_r \alpha_0) = a\delta^2 + b\delta + c \cos(\phi + \phi_0), \quad (\text{A-1})$$

where δ is a canonical momentum, ϕ is a canonical coordinate, z is a canonical time; $\Omega(z)$, u_{\parallel} , f_0 and f'_0 are treated as independent slow-varying parameters.

System dynamics governed by this Hamiltonian has two “time” scales: (a) scale z_{bnc} associated with a particle bounce motion in a homogeneous magnetic field and (b) scale z_{inhom} of explicit dependence of the Hamiltonian on the z coordinate. The analytical treatment can be simplified when a fraction of these two scales ν defined as

$$\nu = \frac{z_{\text{bnc}}}{z_{\text{inhom}}} = \frac{l\Omega' u_{\parallel}}{2\pi k_{\parallel}^2 f_0 J_{l_r}(m\rho/r)}$$

is much greater or much smaller than unity.

When $\nu \gg 1$ one can neglect the term proportional to δ in Eq. (3), omitting nonlinear phase corrections. Particle velocity perturbation change is then given by

$$\Delta\delta \approx - \int \frac{f_0(z) k_z J_{l_r}(m\rho/r)}{u_{\parallel}^0} \cdot \sin \left(\int \frac{\omega - k_z u_{\parallel}^0 - l_r \Omega}{u_{\parallel}^0} dz + l_r \alpha \right) dz. \quad (\text{A-2})$$

Consider a single rf region of a width $l^i \ll L$. Wave-particle resonance occurs in a resonance layer located in a vicinity of $z = z_{\text{res}}$ given by $\omega - k_z u_{\parallel}^0(z_{\text{res}}) - l_r \Omega(z_{\text{res}}) = 0$. Resonance layer width in a configuration space l_{res} can be obtained from Eq. (A-2):

$$l_{\text{res}} \sim \sqrt{\frac{u_{\parallel}}{\Omega'|\chi|}}, \quad (\text{A-3})$$

where $\chi = (l_r - \omega/\Omega)(u_{\perp}^2/2u_{\parallel}^2 - 1) - l_r$. A range of resonant parallel velocities defining diffusion path width in the midplane velocity space is proportional to the difference of magnetic field magnitudes on both sides of the rf region extended by size l_{res} :

$$\Delta u_{\text{res}} \sim \frac{l_r \Omega'(l^i + l_{\text{res}})}{k_z}. \quad (\text{A-4})$$

This expression and the definition of l_{res} suggest that the increase of rf region width over l_{res} increases the range of resonant velocities Δu_{res} , but does not lead to an increase of a wave-particle energy exchange.

When $\nu \ll 1$ and $l^i \ll z_{\text{bnc}}$, Eq. (A-2) can still be used to describe resonant particle interaction. However, when $l^i \gtrsim z_{\text{bnc}}$, trapping and detrapping effects become essential [46–48]. The trapping width [49] $\Delta u_{\text{trap}} \sim \sqrt{f_0 J_l(k_{\perp} \rho)}$ defines the characteristic width of the diffusion path in this regime. The particle velocity change after the passage of the rf region can be estimated by considering adiabatic invariant conservation [50] in both trapped and passing areas of the phase space:

$$J_{\text{passing}} = -\frac{\pi b}{a} \pm \int_0^{2\pi} \xi d\phi = \langle \delta \rangle_{\phi} \approx \text{const},$$

$$J_{\text{trapped}} = \int_{\phi_{\min}}^{\phi_{\max}} \xi d\phi \approx \text{const},$$

where $\xi = \sqrt{b^2 + 4aE - 4ac \cos(\phi + \phi_0)}$ and signs depend on the chosen sheaf of the phase space, ϕ_{\min} and ϕ_{\max} are the minimal and maximal phases for which the integrand turns to zero and $\langle \cdot \rangle_{\phi}$ stands for average over the wave phase.

The particle velocity perturbation evolution in the rf region with smooth profile can be broken into three stages during which adiabatic invariant is approximately conserved: before the trapping, trapping in the wave (if it occurs) and the passing motion after the trapping. If the particle is not trapped in the wave, final value of δ is the same as the initial value

because $\langle \delta \rangle_\phi$ changes when the particle is trapped only. If the particle is trapped in the wave at some point $z = z_t$, depending on parameters and initial particle phase, it can either be reflected from the wave or pass it, untrapping at $z = z_u$ with $\delta = \delta_+ = (-b + \xi)/2a$ or $\delta = \delta_- = (-b - \xi)/2a$, where a , b , c and E are calculated at z_u . It is possible by analogy with Refs. [46–48] to estimate the fractions of reflected and passing particles and the particles detrapping with $\delta = \delta_+$ and $\delta = \delta_-$.

For the magnetic field profiles and rf region parameters employed in the discussed numerical simulations χ was much greater than 1 and thus all the diffusion path characteristics were given by Eqs. (6), (A-3), and (A-4). However, while the detailed calculation of $\langle \Delta\delta \rangle$ and $\langle \Delta\delta^2 \rangle$ in the regime $\chi \ll 1$ lies beyond the scope of this paper, the effect can be estimated by applying the technique discussed in Refs. [44, 45] to the Hamiltonian given by Eq. (A-1).

-
- [1] R. F. Post, Nucl. Fusion Suppl. **1**, 99 (1962).
 - [2] T. K. Fowler, M. Rankin, J. Nucl. Energy **C8**, 121 (1966).
 - [3] N. J. Fisch, J. M. Rax, Phys. Rev. Lett. **69**, 612 (1992).
 - [4] N. J. Fisch, Phys. Rev. Lett. **97**, 225001 (2006).
 - [5] N. J. Fisch, Fusion Sci. Tech. **51(2T)**, 1 (2007).
 - [6] N. J. Fisch, M. C. Herrmann, Nucl. Fusion **35**, 1753 (1995).
 - [7] M. C. Herrmann, N. J. Fisch, Phys. Rev. Lett. **79**, 1495 (1997).
 - [8] N. J. Fisch, M. C. Herrmann, Plasma Phys. Control. Fusion **41**, A221 (1999).
 - [9] R. F. Post, T. K. Fowler, J. Killeen, and A. A. Mirin, Phys. Rev. Lett. **31**, 280 (1973).
 - [10] D. D. Ryutov, in the *Proceedings of the 2nd Wisconsin Symposium on Helium-3 and Fusion Power*, Wisconsin, 1993, compiled by J. F. Santarius (University of Wisconsin, WSCAR-TR-AR3-9307-3, 1993), p. 121.
 - [11] N. J. Fisch, M. C. Herrmann, Nucl. Fusion **34**, 1541 (1994).
 - [12] E. J. Valeo, N. J. Fisch, Phys. Rev. Lett. **73**, 3536 (1994).
 - [13] N. J. Fisch, Phys. Plasmas **2**, 2375 (1995).
 - [14] H. Grawe, Plasma Physics **11**, 151 (1969).
 - [15] J. Kesner, Nucl. Fusion **19**, 108 (1979).

- [16] I. B. Bernstein, D. C. Baxter, Phys. Fluids **24**, 108 (1981).
- [17] A. G. Litvak, A. M. Sergeev, E. V. Suvorov, M. D. Tokman, and I. V. Khazanov, Phys. Fluids B **5**, 4347 (1993).
- [18] D. R. Shklyar, Planet. Space Sci. **34**, 1091 (1986).
- [19] J. M. Albert, Phys. Fluids B **5**, 2744 (1993).
- [20] C. W. Gardiner, in *Handbook of Stochastic Methods for Physics, Chemistry, and the Natural Sciences* (Springer-Verlag New York, LLC, 2004).
- [21] G. R. Smith, N. R. Pereira, Phys. Fluids **21**, 2253 (1978).
- [22] R. E. Aamodt, Phys. Rev. Lett. **27**, 135 (1971).
- [23] M. N. Rosenbluth, Phys. Rev. Lett. **29**, 408 (1972).
- [24] G. R. Smith, J. A. Byers, L. L. Lodestro, Phys. Fluids **23**, 278 (1980).
- [25] C. F. F. Karney, Phys. Fluids **22**, 2188 (1979).
- [26] G. R. Smith, A. N. Kaufman, Phys. Rev. Lett. **34**, 1613 (1975).
- [27] A. Fukuyama, H. Momota, R. Itatani, and T. Takizuka, Phys. Rev. Lett. **38**, 701 (1977)
- [28] T. Intrator, S. Meassick, J. Browning, R. Majeski, J. R. Ferron, and N. Hershkowitz, Nucl. Fusion **29**, 377 (1989).
- [29] Y. Amagishi, A. Tsushima, and M. Inutake, Phys. Rev. Lett. **48**, 1183 (1982).
- [30] R. Majeski, J. J. Browning, S. Meassick, N. Hershkowitz, T. Intrator, and J. R. Ferron, Phys. Rev. Lett. **59**, 206 (1987).
- [31] Y. Yamaguchi, M. Ichimura, H. Higaki, S. Kakimoto, K. Nakagome, K. Nemoto, M. Katano, H. Nakajima, A. Fukuyama, and T. Cho, Plasma Phys. Controlled Fusion **48**, 1155 (2006).
- [32] Y. Yasaka, H. Takeno, A. Fukuyama, T. Toyoda, M. Miyakita, and R. Itatani, Phys. Fluids B **4** (6), 1486 (1992).
- [33] Y. Yamaguchi, M. Ichimura, H. Higaki *et al.*, Journal of Plasma and Fusion Res. **6**, 665 (2004).
- [34] K. Yatsu, T. D. Akhmetov, T. Cho *et al.*, in the *Proceedings of the 28th EPS Conference on Controlled Fusion and Plasma Physics*, Funchal, Portugal, 2001 (The European Physical Society, Geneva, 2001), Vol. **25A**, p. 1549.
- [35] R. Breun, S. N. Golovato, L. Yujiri, B. McVey, A. Molvik, D. Smatlak, R. S. Post, D. K. Smith, and N. Hershkowitz, Phys. Rev. Lett. **47**, 1833 (1981).
- [36] D. E. Baldwin, H. L. Berk, and L. D. Pearlstein, Phys. Rev. Lett. **36**, 1051 (1976).
- [37] W. C. Turner, E. J. Powers, and T. C. Simonen, Phys. Rev. Lett. **39**, 1087 (1977).

- [38] D. E. Baldwin, *Rev. Mod. Phys.* **49**, 317 (1977).
- [39] T. Goto, K. Ishii, Y. Goi, N. Kikuno, Y. Katsuki, M. Yamanashi, M. Nakamura, M. Ichimura, T. Tamano, and K. Yatsu, *Phys. Plasmas* **7**, 2485 (2000).
- [40] T. Cho, J. Kohagura, T. Numakura *et al.*, *Phys. Rev. Lett.* **97**, 055001 (2006).
- [41] V. E. Moiseenko, O. Ågren, *Phys. Plasmas* **12**, 102504 (2005).
- [42] C. Litwin, N. Hershkowitz, *Phys. Fluids* **30**, 1323 (1987).
- [43] J. D. Hanson, E. Ott, *Phys. Fluids* **27**, 150 (1984).
- [44] J. R. Cary, D. F. Escande, and J. L. Tennyson, *Phys. Rev. A* **34**, 4256 (1986).
- [45] J. R. Cary, R. T. Skodje, *Physica D* **36**, 287 (1989).
- [46] D. L. Bruhwiler, J. R. Cary, *Phys. Rev. Lett.* **68**, 255 (1992).
- [47] D. L. Bruhwiler, J. R. Cary, *Phys. Rev. E* **50**, 3949 (1994).
- [48] D. L. Bruhwiler, J. R. Cary, *Part. Accel.* **43**, 195 (1994).
- [49] G. R. Smith, A. N. Kaufman, *Phys. Fluids* **21**, 2230 (1978).
- [50] L. D. Landau, E. M. Lifshitz, in *Mechanics* (Pergamon Press, New York, 1960), p. 154.

The Princeton Plasma Physics Laboratory is operated
by Princeton University under contract
with the U.S. Department of Energy.

Information Services
Princeton Plasma Physics Laboratory
P.O. Box 451
Princeton, NJ 08543

Phone: 609-243-2750
Fax: 609-243-2751
e-mail: pppl_info@pppl.gov
Internet Address: <http://www.pppl.gov>